

# Polarization Switching of Piezoelectric Films due to Proximity of Ferroelectric Nanoclusters

Anna N. Morozovska<sup>1</sup>, Eugene A. Eliseev<sup>2</sup>, Sergei V. Kalin<sup>3</sup>, Long-Qing Chen<sup>4\*</sup>,  
Dean R. Evans<sup>5,6†</sup>, and Venkatraman Gopalan<sup>4‡</sup>

<sup>1</sup> Institute of Physics of the National Academy of Sciences of Ukraine,  
46, Nauki Avenue, 03028 Kyiv, Ukraine

<sup>2</sup>Frantsevich Institute for Problems in Materials Science, National Academy of Sciences of Ukraine,  
3, str. Omeliana Pritsaka, 03142 Kyiv, Ukraine

<sup>3</sup> Department of Materials Science and Engineering, University of Tennessee, Knoxville, TN,  
37996, USA

<sup>4</sup> Department of Materials Science and Engineering,  
Pennsylvania State University, University Park, PA 16802, USA

<sup>5</sup>Zone 5 Technologies, Special Projects Division, San Luis Obispo CA 93401, USA

## Abstract

Using Landau-Ginzburg-Devonshire thermodynamical approach and finite element modelling, we studied the influence of nanoclusters shape on the polarization switching and domain nucleation emerging in otherwise non-switchable piezoelectric films due to the proximity of ferroelectric nanoclusters. The boundary of the ferroelectric nanocluster embedded in the piezoelectric film is a compositionally graded layer. We analyzed the conditions, which allow switching the electric polarization of the piezoelectric AlN film at coercive field significantly lower than the electric breakdown field due to the proximity of ferroelectric  $Al_{1-x}Sc_xN$  clusters. Due to proximity effect, the spontaneous polarization switches in all elements of the nanopatterned film, and corresponding coercive fields can be reduced significantly in the presence of spike-like  $Al_{1-x}Sc_xN$  clusters. We also explored the underlaying physical mechanisms of the proximity effects in the piezoelectric films with ferroelectric nanoclusters. The internal field, which is depolarizing inside the piezoelectric film (due to the larger spontaneous polarization of AlN) and polarizing in the ferroelectric cluster (due to the smaller spontaneous polarization of  $Al_{1-x}Sc_xN$ ), lowers the potential barrier in the clusters and facilitates the instant growth of nanodomains (emerging in the clusters) through the piezoelectric film. Since considered nanostructured materials can be created by implantation of Sc ions into AlN films, obtained theoretical results can be useful for creation of nanopatterned ferroelectrics by chemical engineering, with exciting prospects for previously unrealizable ferroelectric memory technologies.

---

\* corresponding author, e-mail: [lqc3@psu.edu](mailto:lqc3@psu.edu)

† corresponding author, e-mail: [dean.evans92@gmail.com](mailto:dean.evans92@gmail.com)

‡ corresponding author, e-mail: [vgopalan@psu.edu](mailto:vgopalan@psu.edu), [vxg8@psu.edu](mailto:vxg8@psu.edu)

## 1. INTRODUCTION

Nanoscale ferroelectric with wurtzite and fluorite structure are of great scientific interest due to their unique ferroelectric, dielectric, and piezoelectric properties [1, 2, 3]. Recently discovered ferroelectric nitrides and oxides with the wurtzite structure, such as nanoscale *lead-free*  $\text{Al}_{1-x}\text{B}_x\text{N}$ ,  $\text{Al}_{1-x}\text{Sc}_x\text{N}$ ,  $\text{Al}_{1-x}\text{Hf}_x\text{N}$ ,  $\text{Zn}_{1-x}\text{Mg}_x\text{O}$ , and fluoride  $\text{Hf}_x\text{Zr}_{1-x}\text{O}_2$ , are considered to be among the most promising candidates for the next generation of Si-compatible and easily integrable electronic memory elements, such as ferroelectric random access memory (FeRAM), steep-slope field-effect transistors (FETs), various logic devices and piezoelectric actuators [1-3]. These solid-state materials are also chemically and thermally stable, environmentally friendly, have relatively low cost and relatively simple synthesis methods.

The reversal of electric polarization in nitride ferroelectrics is hysteretic with a very high spontaneous polarization (up to  $1.5 - 2 \text{ C/m}^2$ ), but, at the same time, with a very large coercive field, which reaches from 3 to 5 MV/cm for oxides and from 5 to 15 MV/cm for nitrides with a wurtzite structure [4, 5]. These values are close to the electric breakdown fields or exceed them (sometimes several times). The physical reason for the giant spontaneous polarization and anomalously high coercive fields lies in the existence of extremely deep and widely separated potential wells of the free energy of nitride ferroelectrics, which correspond to opposite directions of spontaneous polarization, separated by a high potential barrier [6, 7].

It is known that atomic-scale chemical stresses through bulk doping can stabilize a ferroelectric phase in fluorites (as e.g., in Zr doping of  $\text{HfO}_2$ ) [8]. At the same time, the chemical strain associated with doping can significantly reduce the height of the free energy potential barriers and thus reduce the coercive field of polarization switching to practically acceptable values [9, 10, 11]. For example, the barrier is lowered both when doping the polar but non-switchable piezoelectric zinc oxide ( $\text{ZnO}$ ) with magnesium [12], and when doping the polar but non-switchable aluminum nitride ( $\text{AlN}$ ) with scandium or boron [13, 14]. However, doping, as a rule, has a detrimental effect on other functional properties of wurtzite ferroelectrics, such as dielectric losses and electrochemical activity [15], significant optical scattering losses that impede optoelectronic and/or other applications [16]. A question arises as to whether it is possible to apply such stress only at/near the surfaces of an otherwise non-switchable polar material to trigger ferroelectric switching without breakdown.

Emerging ideas are to exploit size effects and “proximity to the ferroelectric” of an otherwise non-switchable ferroelectric to induce ferroelectric switching of  $\text{AlN}$  and  $\text{ZnO}$  piezoelectrics without their electrical breakdown [17]. Polarization reversal has been experimentally observed in  $\text{AlN}$  and  $\text{ZnO}$  piezoelectric layers, which were in direct electric contact with “chemically related” ferroelectric layers, such as  $\text{Al}_{1-x}\text{B}_x\text{N}$ ,  $\text{Al}_{1-x}\text{Sc}_x\text{N}$ , and  $\text{Zn}_{1-x}\text{Mg}_x\text{O}$ , in multilayer films. The layered structures, whose thicknesses varied from tens to hundreds of nm, included two-layer (asymmetric, e.g.  $\text{Al}_{1-x}\text{B}_x\text{N}/\text{AlN}$ ), three-layer ( $\text{Al}_{1-x}\text{B}_x\text{N}/\text{AlN}/\text{ZnO}$ ), and four-layer ( $\text{Al}_{1-x}\text{B}_x\text{N}/\text{AlN}/\text{ZnO}/\text{Al}_{1-x}\text{B}_x\text{N}$ ) configurations.

$\text{xSc}_x\text{N}/\text{AlN}$ ,  $\text{Al}_{1-x}\text{B}_x\text{N}/\text{AlN}$ ,  $\text{ZnO}/\text{Al}_{1-x}\text{B}_x\text{N}$ ) and three-layer (symmetric, e.g.  $\text{Al}_{1-x}\text{B}_x\text{N}/\text{AlN}/\text{Al}_{1-x}\text{B}_x\text{N}$ ,  $\text{AlN}/\text{Al}_{1-x}\text{B}_x\text{N}/\text{AlN}$ ,  $\text{Zn}_{1-x}\text{Mg}_x\text{O}/\text{ZnO}/\text{Zn}_{1-x}\text{Mg}_x\text{O}$ ) configurations [17]. The first attempts of the “proximity to the ferroelectric” thermodynamic description in wurtzite multilayer structures are presented in Refs. [18, 19].

Compositionally graded ferroelectric materials can be imagined as the natural limit of multilayer structures under the layer thickness decrease. Prof. Alpay group [20, 21, 22, 23], who developed a generalized Landau-Ginzburg-Devonshire (LGD) approach for analyzing compositionally graded ferroelectric nanomaterials, revealed the leading role of compositional strain and stress gradients in the formation of domain structures and polarization reversal by applied electric field, thus proposed avenues for versatile advanced applications of the nanomaterials.

As was recently discovered, the compositionally graded planar structures  $\text{AlN}-\text{Al}_{1-x}\text{Sc}_x\text{N}$  and  $\text{ZnO}-\text{Zn}_{1-x}\text{Mg}_x\text{O}$  allow the simultaneous switching of spontaneous polarization in the whole system by a coercive field significantly lower than the electric breakdown field of unswitchable polar materials [24]. The physical mechanism is the depolarization electric field determined by the gradient of chemical composition “x”, that lowers the steepness of the switching barrier in the otherwise unswitchable parts of the compositionally graded structures [24]. These results indicate that silicon-compatible compositionally graded wurtzite ferroelectrics can be very promising for advanced nanoelectronics, optoelectronics and related emerging technologies.

However, to the best of our knowledge, polar and electrophysical properties of compositionally graded wurtzite nanoclusters and nanoparticles have not been studied. Methods for controlling these properties by changing the chemical composition gradient, shape and size effects, and/or proximity effects have not been developed. There is a scientific and practical interest for creating wurtzite nanomaterials with high spontaneous polarization and significantly reduced coercive fields, which can be controlled by chemical and physical factors.

To fill the gap in knowledge, in this work we analyze theoretically the influence of nanocluster shape on the polarization switching and domain nucleation emerging in otherwise non-switchable piezoelectric films due to the proximity of ferroelectric nanoclusters. The boundary of the ferroelectric nanocluster in the piezoelectric film is a compositionally graded layer. Using LGD thermodynamical approach and finite element modelling (FEM), we analyze the conditions, which allow switching the electric polarization of the piezoelectric AlN film at coercive field significantly lower than the electric breakdown field due to the proximity of ferroelectric  $\text{Al}_{1-x}\text{Sc}_x\text{N}$  clusters. We also explore the underlying physical mechanisms of the proximity effects in the piezoelectric films with ferroelectric nanoclusters.

## 2. PROBLEM FORMULATION

Let us consider switchable ferroelectric  $\text{Al}_{1-x}\text{Sc}_x\text{N}$  nanoclusters embedded in the otherwise non-switchable AlN film covered by conducting electrodes (shown in **Fig. 1(a)**). The XZ cross-section of the clusters has the width is  $2R$  and the height is  $d$ . The clusters are regarded as wires in the third direction Y, that allows us to solve quasi-2D problem. The boundary between the  $\text{Al}_{1-x}\text{Sc}_x\text{N}$  clusters and the AlN material is a compositionally graded layer, whose thickness is determined by the diffusion length  $\Delta$  and preparation/implantation conditions. The thickness of AlN film is  $h$ . The period  $L$  between the clusters coincides with the lateral size of the computational cell. For comparison, we consider the inverted structure, namely the AlN nanoclusters in the  $\text{Al}_{1-x}\text{Sc}_x\text{N}$  film covered by electrodes (shown in **Fig. 1(b)**).

An electric voltage  $U(t)$  is applied to the top electrode (its electric potential  $\varphi = U(t)$ ). The voltage amplitude increases linearly in time from zero to  $U_{max}$ , namely  $U(t) = U_{max} \frac{t}{t_{max}} \sin(\omega t)$ , where  $\omega$  is the pulse frequency and  $t_{max}$  is the computation time. Such form of the voltage sweep corresponds to existing experiments [12, 15] and allows us to study different stages of polarization reversal [18, 19, 24] in the clusters and in the film. The bottom electrode is regarded as electrically grounded (its electric potential  $\varphi = 0$ ).

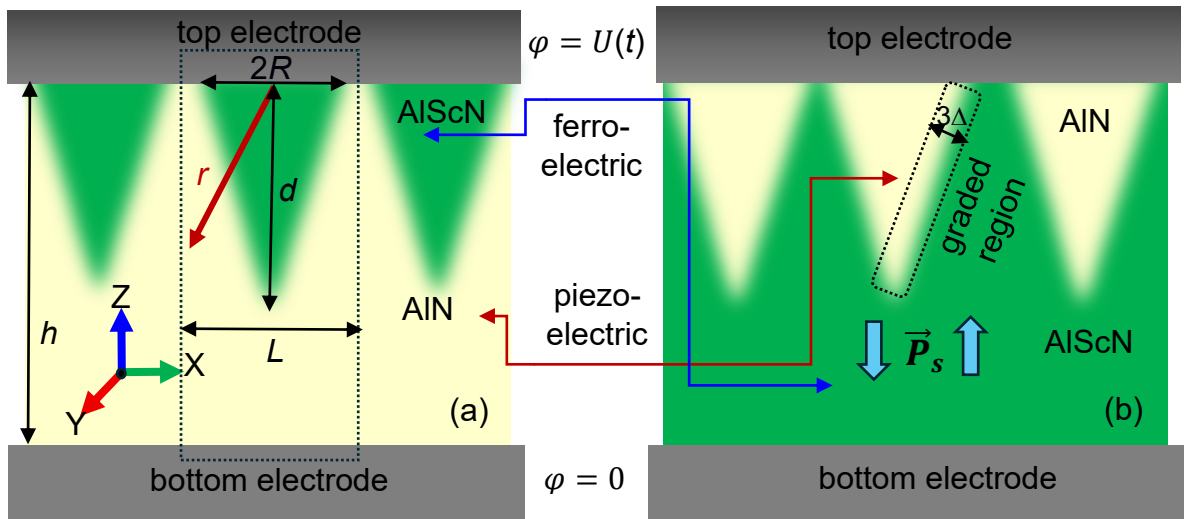


**FIGURE 1.** (a)  $\text{Al}_{1-x}\text{Sc}_x\text{N}$  nanoclusters in the AlN film, and (b) AlN nanoclusters in the  $\text{Al}_{1-x}\text{Sc}_x\text{N}$  film, placed between the parallel-plate electrodes. The boundary between the  $\text{Al}_{1-x}\text{Sc}_x\text{N}$  and AlN is a compositionally graded layer with effective thickness about  $3\Delta$ . The cluster width is  $2R$  and its height is  $d$ . The clusters are regarded as wires in the third direction Y, which is perpendicular to the figure plane. The film thickness is  $h$ . A polar c-axis of wurtzite is normal to the electrode surfaces and coincides with Z-axis. Dotted rectangle in part (a) shows the lateral size  $L$  of the computational cell. Two directions of the out-of-plane spontaneous polarization  $\vec{P}_s$  are shown by thick arrows in part (b).

Our goal is to find the conditions (e.g., the optimal shape, sizes  $R$  and  $d$ , of the ferroelectric nanoclusters, the diffusion length  $\Delta$  and the cluster period  $L$ ), which allows switching the spontaneous polarization of the piezoelectric film at coercive field significantly lower than the electric breakdown field due to the proximity effect. It is also interesting to study the appearance of proximity effects in the inverted structure for different parameters  $R$ ,  $d$ ,  $\Delta$  and  $L$ .

The time-dependent LGD equation for the ferroelectric polarization  $P_z$  inside a compositionally graded wurtzite nanocluster is the following:

$$\Gamma \frac{\partial P_z}{\partial t} + \alpha(\vec{r})P_z + \beta(\vec{r})P_z^3 + \gamma(\vec{r})P_z^5 - g_z \frac{\partial^2 P_z}{\partial z^2} - g_{\perp} \Delta_{\perp} P_z = E_z. \quad (1a)$$

Here  $\Gamma$  is the Landau-Khalatnikov relaxation coefficient;  $\Delta_{\perp}$  is the transverse part of Laplace operator,  $E_z = -\frac{\partial \varphi}{\partial z}$  is z-component of electric field. The Landau expansion coefficients  $\alpha$ ,  $\beta$  and  $\gamma$  are coordinate-dependent due to the gradient of the chemical composition “x” in the following way:

$$\alpha(\vec{r}) = \alpha_1 + (\alpha_2 - \alpha_1) \exp\left(-\frac{|\vec{r} - \vec{r}_S|}{\Delta}\right) - 2Q_{13}(\vec{r})(\sigma_{22} + \sigma_{11}) - 2Q_{33}(\vec{r})\sigma_{33}, \quad (1b)$$

$$\beta(\vec{r}) = \beta_1 + (\beta_2 - \beta_1) \exp\left(-\frac{|\vec{r} - \vec{r}_S|}{\Delta}\right), \quad \gamma(\vec{r}) = \gamma_1 + (\gamma_2 - \gamma_1) \exp\left(-\frac{|\vec{r} - \vec{r}_S|}{\Delta}\right). \quad (1c)$$

Here  $\vec{r}$  is the radius-vector counted from the cluster center, the radius-vector  $\vec{r}_S$  describe its surface, and the diffusion length  $\Delta$  determines the thickness of the graded layer. The coefficients  $\alpha_1$ ,  $\beta_1$  and  $\gamma_1$  correspond to the ferroelectric  $\text{Al}_{0.73}\text{Sc}_{0.27}\text{N}$ ; the coefficients  $\alpha_2$ ,  $\beta_2$  and  $\gamma_2$  correspond to the piezoelectric  $\text{AlN}$  for the structure shown in **Fig. 1(a)** (or vice versa for the structure shown in **Fig. 1(b)**). The coefficient  $\alpha(\vec{r})$  is renormalized by elastic stresses  $\sigma_{ij}$  via the electrostriction coefficients  $Q_{ij}$ . For the sake of simplicity, we regard that elastic constants are the same in both materials. Elastic stresses satisfy the equation of mechanical equilibrium in the computation region,  $\frac{\partial \sigma_{ij}}{\partial x_j} = 0$ . Elastic equations of state follow from the variation of the free energy with respect to elastic stress, namely:

$$S_{ijkl}\sigma_{ij} + Q_{ijkl}P_k P_l = u_{ij}. \quad (1c)$$

Elastic boundary conditions correspond to the absence of normal stress at the top electrode ( $z = h$ ) and zero elastic displacement at the bottom electrode ( $z = 0$ ) due to the rigid substrate. Hereafter, we neglect the influence of the flexoelectric coupling for the sake of simplicity.

For this work, we regard polarization and its derivatives are continuous functions inside the nanostructured film. The boundary conditions for polarization at the top ( $z = h$ ) and bottom ( $z = 0$ ) surfaces of the film are of the third type [25]:

$$\frac{\partial P_z}{\partial z} - \frac{P_z}{\lambda_1} = 0 \Big|_{z=0}, \quad \frac{\partial P_z}{\partial z} + \frac{P_z}{\lambda_2} = 0 \Big|_{z=h}, \quad (2)$$

where  $\lambda_1$  and  $\lambda_2$  are the so-called extrapolation lengths [26], whose values depend on the surface-electrode pair, the nature of the short-range interactions at the surface/interface and/or preparation conditions, being the model/fitting parameters. The limiting case  $\lambda_i \rightarrow 0$  corresponds to zero polarization at the surface and favors the domain formation under the incomplete screening conditions. The limiting case  $\lambda_i \rightarrow \infty$ , used in this work, corresponds to the so-called natural boundary conditions, which maximally support the single-domain state of the film covered with ideally conducting electrodes.

The electric potential  $\varphi$  obeys the Poisson equation,  $\varepsilon_0 \frac{\partial}{\partial x_i} \left[ \varepsilon_{ij}(\vec{x}) \frac{\partial}{\partial x_j} \varphi(\vec{x}) \right] = \frac{\partial P_k(\vec{x})}{\partial x_k}$ . Since the wurtzite structures are considered as uniaxial ferroelectrics with the polar axis Z, we regard that the in-plane components of polarization have the form:

$$P_1(\vec{r}) = -\varepsilon_0 [\varepsilon_{11}(\vec{r}) - 1] \frac{\partial \varphi}{\partial x}, \quad P_2(\vec{r}) = -\varepsilon_0 [\varepsilon_{11}(\vec{r}) - 1] \frac{\partial \varphi}{\partial y}, \quad (3a)$$

where the function  $\varepsilon_{11}(\vec{r}) = \varepsilon_{11}^{(1)} + (\varepsilon_{11}^{(2)} - \varepsilon_{11}^{(1)}) \exp\left(-\frac{|\vec{r} - \vec{r}_S|}{\Delta}\right)$ ,  $\varepsilon_{11}^{(1)}$  and  $\varepsilon_{11}^{(2)}$  are in-plane dielectric permittivities;  $\varepsilon_0$  is a universal dielectric constant. The out-of-plane component of polarization has the form:

$$P_3(\vec{r}) = P_z(\vec{r}) - \varepsilon_0 [\varepsilon_b(\vec{r}) - 1] \frac{\partial \varphi}{\partial z}, \quad (3b)$$

where  $P_z(\vec{r})$  is the ferroelectric/piezoelectric part of polarization related with the soft mode; the function  $\varepsilon_b(\vec{r}) = \varepsilon_b^{(1)} + (\varepsilon_b^{(2)} - \varepsilon_b^{(1)}) \exp\left(-\frac{|\vec{r} - \vec{r}_S|}{\Delta}\right)$ ,  $\varepsilon_b^{(1)}$  and  $\varepsilon_b^{(2)}$  correspond to the background permittivity [27] of ferroelectric and piezoelectric materials, respectively. From Eqs.(3a) and (3b), the Poisson equation acquires the form:

$$\varepsilon_0 \left[ \varepsilon_{11}(\vec{r}) \Delta_{\perp} \varphi + \frac{\partial}{\partial z} \left( \varepsilon_b(\vec{r}) \frac{\partial \varphi}{\partial z} \right) \right] = \frac{\partial P_z}{\partial z}. \quad (4a)$$

The electric boundary conditions are the fixed potential at the electrodes,

$$\varphi|_{z=0} = 0, \quad \varphi|_{z=h} = U(t). \quad (4b)$$

LGD parameters of  $\text{Al}_{0.73}\text{Sc}_{0.27}\text{N}$  and AlN, used in our calculations, are listed in **Table SI** in Supplementary Materials [28]. They are determined from Refs. [4, 5, 29, 30]. Electrostriction coefficients  $Q_{ij}$  and elastic stiffness tensors  $c_{ij}$ , listed in **Tables S2** [28], are taken from Refs. [6, 31]. The procedure for the determination of LGD parameters and constitutive equations, solved by FEM, are described in detail in Refs. [18, 19, 24].

We perform the FEM in COMSOL@MultiPhysics software, using electrostatics, solid mechanics, and general math (PDE toolbox) modules, for different discretization densities of the rectangular mesh and polarization relaxation conditions. The maximal size of the quasi 2D-computational region is equal to  $L \times h \times D \text{ nm}^3$ , where the distance D in the Y-direction can be small enough due to the independence of all physical properties on the coordinate “y”. The diffusion length

$\Delta$  changes from 1 to 5 nm, at the period  $L$  is taken several times larger than the cluster size. Periodic boundary conditions are imposed in Y-direction and at lateral boundaries of the computational cell. The average size of the mesh element is equal to 0.5 nm. The physical properties dependence on the mesh size is verified by increasing the size to 1.0 nm. We found that this results in minor changes in the electric polarization, electric field, and elastic stresses and strains, such that the spatial distribution of each of these quantities becomes less smooth. When using these larger cell sizes, all significant details remain visible, and, more importantly, the system free energy saturates with the mesh size decrease below 1 nm.

### 3. RESULTS AND DISCUSSION

To find the conditions, which allows switching the spontaneous polarization of the piezoelectric AlN film at coercive field significantly lower than the electric breakdown field, we vary the shape of  $\text{Al}_{0.73}\text{Sc}_{0.27}\text{N}$  clusters by changing the aspect ratio  $R/d$  at fixed area of the cluster cross-section,  $S = \pi R d / 2$  (see schematics in **Fig. 2(a)**). To study the clusters role as polar defects, we consider the case, when their relative volume fraction  $v_c = S/(hL)$  is small, namely  $v_c \leq 0.1$ . For comparison we consider the polarization switching in  $\text{Al}_{0.73}\text{Sc}_{0.27}\text{N}/\text{AlN}$  bilayer structure separated by the compositionally graded layer, as well as in the vertical  $\text{Al}_{0.73}\text{Sc}_{0.27}\text{N}$ –AlN striped structure, which are shown schematically in **Fig. 2(b)** and **2(c)**, respectively. The thickness of the  $\text{Al}_{0.73}\text{Sc}_{0.27}\text{N}$  layer  $d$  and the width of  $\text{Al}_{0.73}\text{Sc}_{0.27}\text{N}$  stripes  $w$  are chosen so that their volume fractions,  $v_{bl} = \frac{d}{h}$  and  $v_{st} = \frac{wh}{L^2}$ , are the same as  $v_c$ .

**Figure 2(d)** shows the polarization-voltage hysteresis loops  $\bar{P}_z(U)$  calculated for different cross-section shapes of  $\text{Al}_{0.73}\text{Sc}_{0.27}\text{N}$  nanoclusters in the AlN film, and **Fig. 2(e)** shows the  $\bar{P}_z(U)$  loops calculated for different cross-section shapes of AlN nanoclusters in the  $\text{Al}_{0.73}\text{Sc}_{0.27}\text{N}$  film. **Figure 3** illustrates the features of polarization switching in the structure consisting of spike-like  $\text{Al}_{0.73}\text{Sc}_{0.27}\text{N}$  nanoclusters ( $R \ll d$ ) periodically spaced in the AlN film. **Figure 4** illustrates the features of polarization switching in the inverted structure consisting of semi-circular AlN nanoclusters ( $R = d$ ) periodically spaced in the  $\text{Al}_{0.73}\text{Sc}_{0.27}\text{N}$  film.

Results, shown in various panels of **Figs. 2–4**, are calculated in the case of a single-domain initial distribution of polarization in nanostructured films. Specifically, the initial state was an upward-directed spontaneous polarization with random small fluctuations in all layers. Note that the single-domain state of the spontaneous polarization is the ground state of the nanostructured films, since the surface screening is regarded ideal, and the boundary condition  $\varphi = 0$  is valid at both surfaces. We waited until the initial spontaneous polarization relaxed to a single-domain state and then applied the voltage according to the same timing protocol (shown in **Figs. 3(a)** and **4(a)**).

Due to proximity effect, the spontaneous polarization switches simultaneously in all elements for all considered geometries, and corresponding coercive fields depend significantly on the geometry. From comparison of the width of  $P_3(U)$  loops in **Fig. 2(d)** one can conclude the following. The inclusion of spike-like  $\text{Al}_{0.73}\text{Sc}_{0.27}\text{N}$  clusters (or stripes) reduces the coercive field of the AlN film strongest of all ( $\sim 1.56$  times compared to pure AlN film). The inclusion of semi-circular  $\text{Al}_{0.73}\text{Sc}_{0.27}\text{N}$  clusters leads to smaller reduction of the coercive field; and the inclusion of flattened  $\text{Al}_{0.73}\text{Sc}_{0.27}\text{N}$  clusters (or horizontal layer) reduces the coercive field weakest of all ( $\sim 1.04$  times compared to AlN film). The remanent polarization,  $P_r \approx \pm 122 \mu\text{C}/\text{cm}^2$ , is close to the polarization of a bulk AlN. The magnitude of  $P_r$  is almost independent on the cluster shape, because the relative volume fraction  $\nu_c$  of the clusters is small, namely  $\nu_c \approx \pi/40$ .

The impact of the spike-like clusters on the resulting coercive field is the strongest, because the internal electric field, which tends to minimize the difference in spontaneous polarization of the AlN and  $\text{Al}_{0.73}\text{Sc}_{0.27}\text{N}$  materials [18, 19, 24], is concentrated near the bottom end of the spike (see **Fig. 2(f)**). In result, nanodomains nucleate inside the  $\text{Al}_{0.73}\text{Sc}_{0.27}\text{N}$  spikes at lower voltages in comparison with other shapes of the clusters. The internal field, which is depolarizing inside the piezoelectric film (due to the larger spontaneous polarization of a bulk AlN material,  $P_{\text{AlN}} \approx 126 \mu\text{C}/\text{cm}^2$ ) and polarizing in the ferroelectric cluster (due to the smaller spontaneous polarization of a bulk  $\text{Al}_{0.73}\text{Sc}_{0.27}\text{N}$  material,  $P_{\text{AlScN}} \approx 105 \mu\text{C}/\text{cm}^2$ ), lowers the potential barrier in the clusters and facilitates the instant vertical growth of the nanodomains towards the bottom electrode. More slow lateral growth of the domain stripes starts in the piezoelectric film after that. The scenario of nanodomain nucleation and growth is illustrated by the images in **Fig. 3(f)**. The images 1 – 8 show the distribution of  $P_z$  in the cross-section of the nanostructures films at the moments of time numbered from “1” to “8” in the voltage sweep, shown in **Figs. 3(a)**. The time sweeps of the averaged polarization  $\bar{P}_z$  and vertical surface displacement  $u_z$ , corresponding to the voltage sweep, are shown in **Fig. 3(b)** and **Fig. 3(c)**, respectively. The ferroelectric hysteresis loops of the averaged  $\bar{P}_z$  and the butterfly-like loops of the  $u_z$  are shown in **Figs. 3(d)** and **3(e)**, respectively.

Note that the coercive fields of the AlN films with spike-like and striped  $\text{Al}_{0.73}\text{Sc}_{0.27}\text{N}$  clusters are very close (compare blue and green curves in **Fig. 2(d)**). The conditions of domain nucleation are less favorable for circular and flattened cross-sections of the clusters, because the polarizing field inside the  $\text{Al}_{0.73}\text{Sc}_{0.27}\text{N}$  clusters are smaller in the case (see **Fig. 2(g)** and **2(h)**), requiring higher coercive fields to switch the spontaneous polarization of the film.

We also analyzed the polarization switching in the inverted structures, where we varied the shape of AlN clusters in the  $\text{Al}_{0.73}\text{Sc}_{0.27}\text{N}$  film. Corresponding  $P_3(U)$  loops are shown in **Fig. 2(e)**. We revealed that the clusters with semi-circular cross-section reduce the coercive field strongest of all other shapes of the cross-sections. The coercive fields of the  $\text{Al}_{0.73}\text{Sc}_{0.27}\text{N}$  film with flattened or

semi-circular AlN clusters appear smaller (up to  $\sim 1.22$  times) than the field of a pure  $\text{Al}_{0.73}\text{Sc}_{0.27}\text{N}$  film without clusters. This result seems counterintuitive, but it can be explained by the distribution of internal electric field in the structure. The internal field emerges to minimize the difference in spontaneous polarization of the  $\text{Al}_{0.73}\text{Sc}_{0.27}\text{N}$  and AlN materials [18, 19, 24]. The impact of the flattened or semi-circular AlN clusters on the resulting coercive field is the strongest, because the internal electric field is concentrated near the contact of the clusters with the top electrode (see **Fig. 2(j)** and **2(k)**). In result, nanodomains nucleate outside the AlN clusters, in the immediate vicinity of cluster-electrode contacts, which act as polar interfacial defects. Due to the local interfacial enhancement of polarization and field [32], nucleation starts at lower voltages in comparison with other shapes of the clusters (which are also lower in comparison with the film without interfacial defects). The internal field, which is polarizing inside the ferroelectric film (due to the smaller spontaneous polarization of  $\text{Al}_{0.73}\text{Sc}_{0.27}\text{N}$ ) and depolarizing in the piezoelectric cluster (due to the larger spontaneous polarization of AlN), lowers the potential barrier in the film and facilitates the nucleation of nanodomains near the polar interfacial defects. Next stages are the vertical growth of needle-like nanodomains towards the bottom electrode and their further lateral growth in the film and in the AlN clusters due to the proximity effect. The scenario of nanodomain nucleation and growth is illustrated by the images in **Fig. 4(f)**. The images 1 – 10 show the distribution of  $P_z$  in the cross-section of the nanostructures films at the moments of time numbered from “1” to “10” in the voltage sweep, shown in **Figs. 4(a)**. The time sweeps of the averaged polarization  $\bar{P}_z$  and vertical surface displacement  $u_z$ , corresponding to the voltage sweep, are shown in **Fig. 4(b)** and **Fig. 4(c)**, respectively. The ferroelectric hysteresis loops of the averaged  $\bar{P}_z$  and the butterfly-like loops of the  $u_z$  are shown in **Figs. 4(d)** and **4(e)**, respectively.

Note the coercive fields of the  $\text{Al}_{0.73}\text{Sc}_{0.27}\text{N}$  films with the semi-circular and flattened AlN clusters are close; both fields are smaller than the coercive field of a pure  $\text{Al}_{0.73}\text{Sc}_{0.27}\text{N}$  film (compare magenta and dotted scarlet curves in **Fig. 2(e)**). The conditions of domain nucleation are less favorable for the spike-like cross-section of the clusters, because the polarizing field outside the AlN clusters are smaller in the case (see **Fig. 2(i)**), requiring slightly higher coercive fields to switch the spontaneous polarization of the  $\text{Al}_{0.73}\text{Sc}_{0.27}\text{N}$  film (compare blue, green and dashed black curves in **Fig. 2(e)**). The largest coercive field corresponds to the AlN/ $\text{Al}_{0.73}\text{Sc}_{0.27}\text{N}$  bilayer structure (see the red curve in **Fig. 2(e)**).

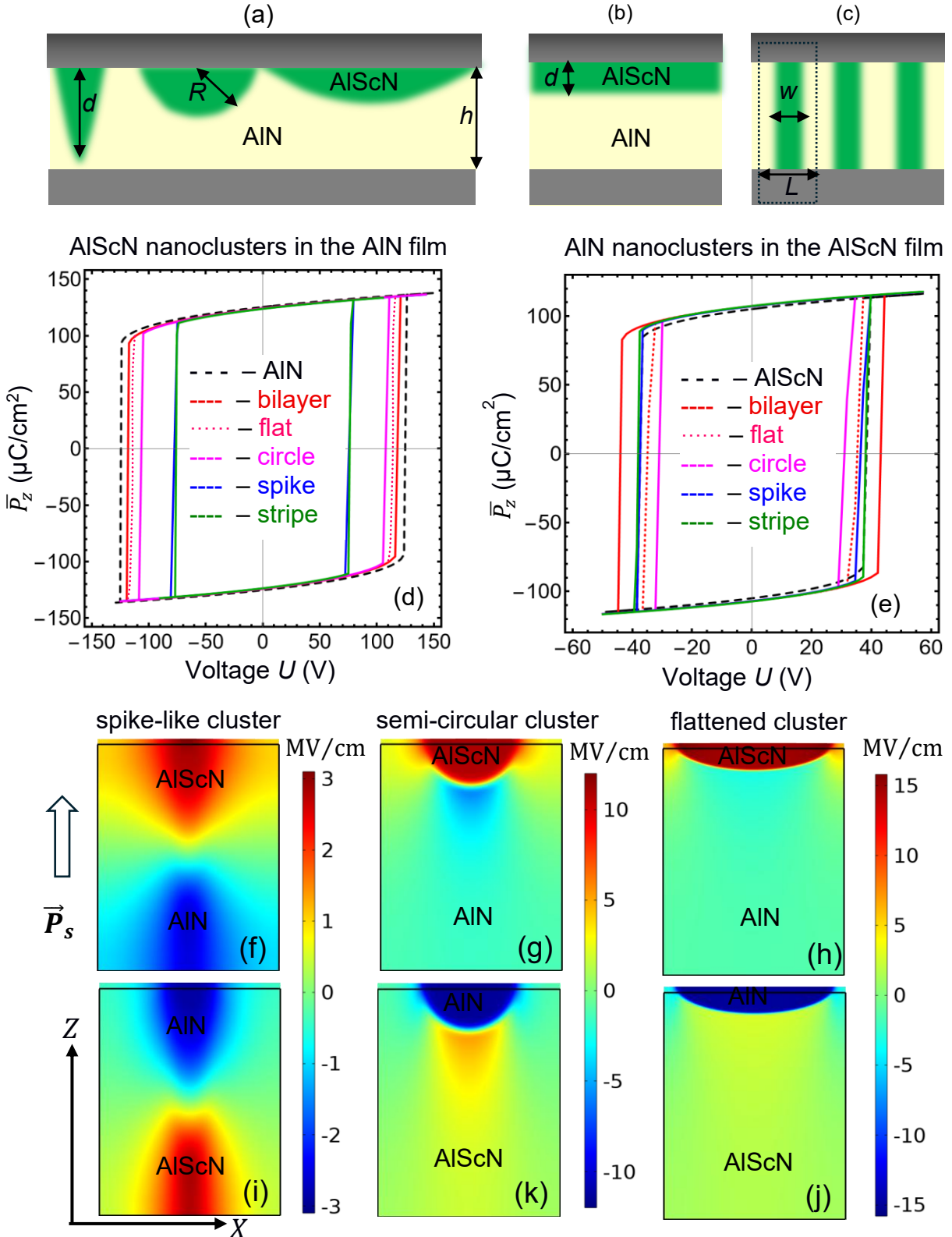


**FIGURE 2.** (a) Considered cross-sections of the Al<sub>1-x</sub>Sc<sub>x</sub>N clusters: spike-like, semi-circular and flattened shape. (b) Horizontal bilayer Al<sub>1-x</sub>Sc<sub>x</sub>N/AlN and (c) vertical striped Al<sub>1-x</sub>Sc<sub>x</sub>N-AlN nanostructures. (d) Polarization-voltage hysteresis loops  $\bar{P}_z(U)$  calculated for different cross-section shapes of Al<sub>0.73</sub>Sc<sub>0.27</sub>N nanoclusters in the AlN film, placed between the parallel-plate electrodes. (e)  $\bar{P}_z(U)$  loops calculated for different cross-section shapes of AlN nanoclusters in the Al<sub>0.73</sub>Sc<sub>0.27</sub>N film, placed between the parallel-plate electrodes. Black dashed loops correspond to the pure AlN (or Al<sub>0.73</sub>Sc<sub>0.27</sub>N) film, red loops correspond to the

4 nm  $\text{Al}_{0.73}\text{Sc}_{0.27}\text{N}$  / 46 nm AlN (or 46 nm AlN / 4 nm  $\text{Al}_{0.73}\text{Sc}_{0.27}\text{N}$ ) bilayers, scarlet dotted loops correspond to the flattened  $\text{Al}_{0.73}\text{Sc}_{0.27}\text{N}$  (or AlN) clusters with sizes  $R = 17.2$  nm and  $d = 5.8$  nm, magenta loops correspond to the semi-circular  $\text{Al}_{0.73}\text{Sc}_{0.27}\text{N}$  (or AlN) clusters with cross-section radius  $R = 10$  nm, blue loops correspond to the spike-like  $\text{Al}_{0.73}\text{Sc}_{0.27}\text{N}$  (or AlN) clusters with cross-section sizes  $R = 4$  nm and  $d = 25$  nm, and green loops correspond to the  $\text{Al}_{0.73}\text{Sc}_{0.27}\text{N}$  (or AlN) vertical stripes of 1.6 nm thick in the AlN (or  $\text{Al}_{0.73}\text{Sc}_{0.27}\text{N}$ ) film. Distribution of internal electric field in the AlN film with spike-like (**f**), semi-circular (**g**) and flattened (**h**)  $\text{Al}_{0.73}\text{Sc}_{0.27}\text{N}$  nanoclusters calculated at  $U = 0$ . Distribution of internal electric field in the  $\text{Al}_{0.73}\text{Sc}_{0.27}\text{N}$  film with spike-like (**i**), semi-circular (**j**) and flattened (**k**) AlN nanoclusters calculated at  $U = 0$ . White arrow shows the direction of spontaneous polarization. The film thickness  $h = 50$  nm, the cluster cross-section is fixed as  $50\pi$  nm $^2$ , the diffusion length  $\Delta = 3$  nm, and the lateral period of the structure is  $L = 40$  nm. LGD parameters and elastic constants are listed in **Tables S1** and **S2**.

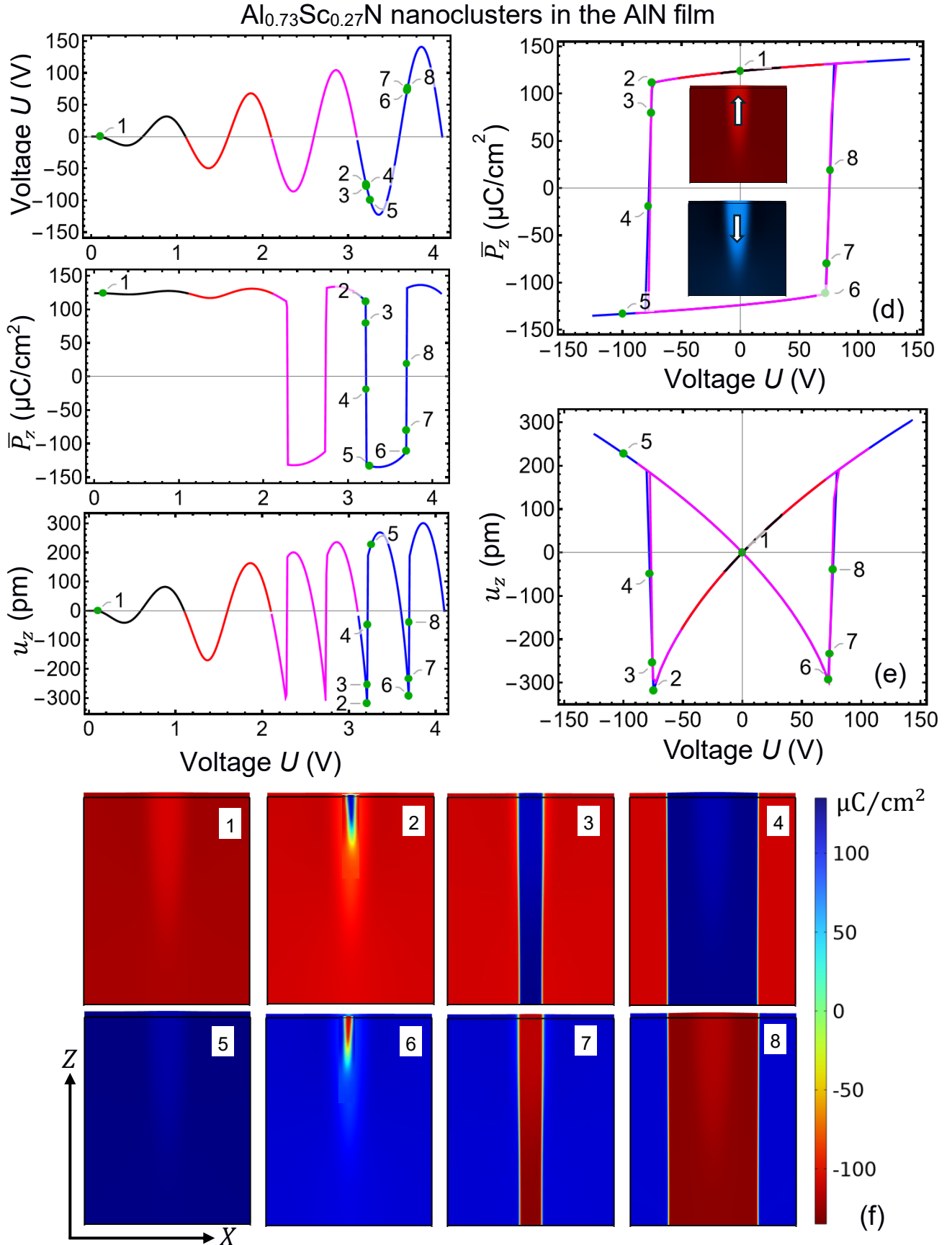


**FIGURE 3.** Time dependences of the electric voltage applied between the electrodes **(a)**, the average polarization  $\bar{P}_z$  **(b)** and the vertical displacement  $u_z$  of the top surface **(c)** in the structure consisting of Al<sub>0.73</sub>Sc<sub>0.27</sub>N nanoclusters with the spike-like cross-section, which are periodically spaced in the AlN film.

Voltage dependences of the average polarization  $\bar{P}_z$  (d) and surface displacement  $u_z$  (e). (g) The distribution of polarization  $P_z$  in the XZ-section of the structure at the moments of time numbered from “1” to “8” shown by the pointers in the part (a). The film thickness  $h = 50$  nm, the cluster sizes  $R = 4$  nm and  $d = 25$  nm, the diffusion length  $\Delta = 3$  nm, and the lateral period of the structure is  $L = 40$  nm. LGD parameters and elastic constants are listed in **Tables S1** and **S2**.

### AlN nanoclusters in the $\text{Al}_{0.73}\text{Sc}_{0.27}\text{N}$ film

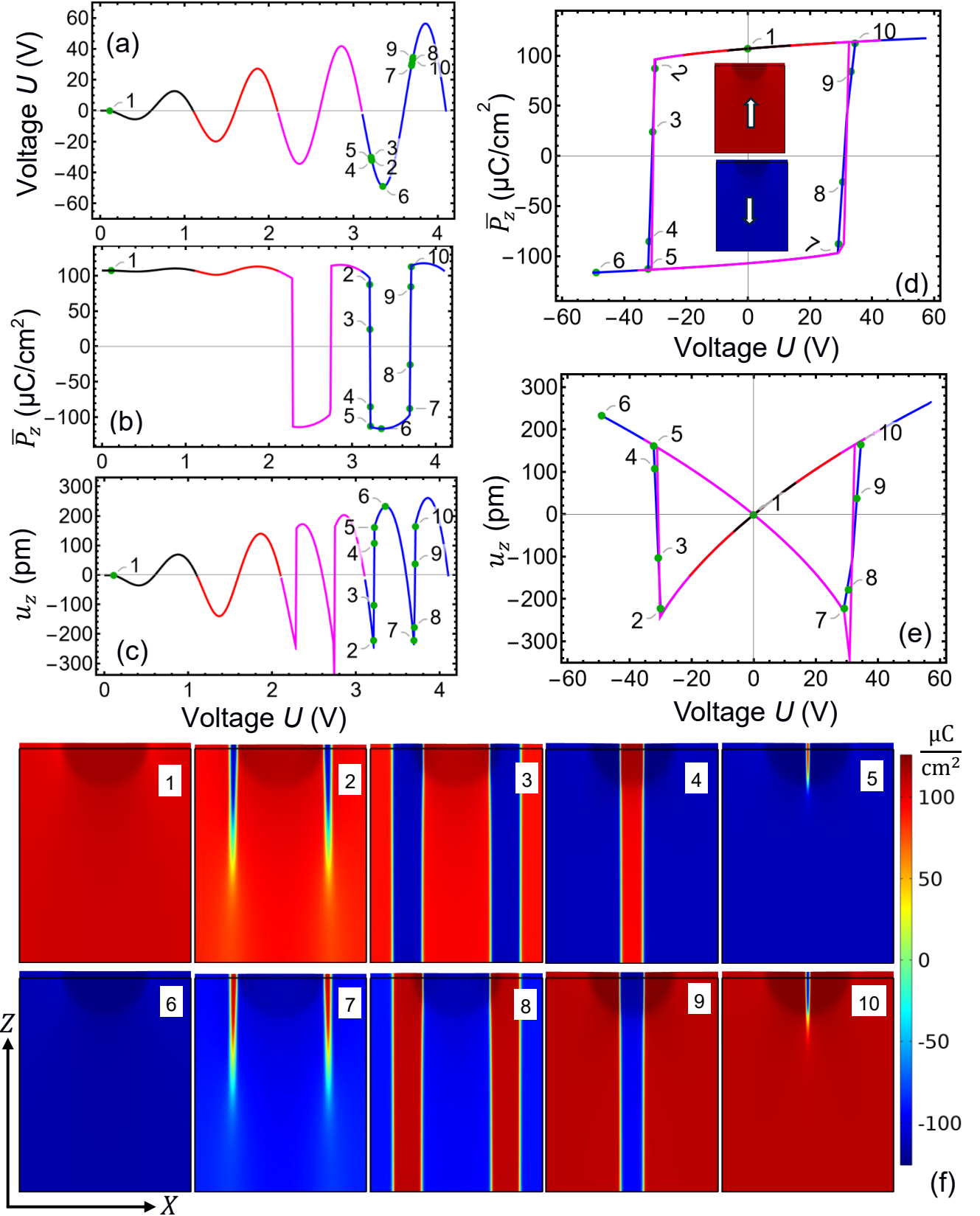


**FIGURE 4.** Time dependences of the electric voltage applied between the electrodes **(a)**, the average polarization  $\bar{P}_z$  **(b)** and the vertical displacement  $u_z$  of the top surface **(c)** in the structure consisting of AlN nanoclusters with semi-circular cross-section, which are periodically spaced in the  $\text{Al}_{0.73}\text{Sc}_{0.27}\text{N}$  film. Voltage dependences of the average polarization  $\bar{P}_z$  **(d)** and surface displacement  $u_z$  **(e)**. **(g)** The distribution of

polarization  $P_z$  in the XZ-section of the structure at the moments of time numbered from “1” to “10” shown by the pointers in the part (a). The film thickness  $h = 50$  nm, the cluster sizes  $R = 10$  nm and  $d = 10$  nm, the diffusion length  $\Delta = 3$  nm, and the lateral period of the structure is  $L = 40$  nm. LGD parameters and elastic constants are listed in **Tables S1** and **S2**.

#### 4. CONCLUSION

Using Landau-Ginzburg-Devonshire thermodynamical approach and finite element modelling, we studied the influence of nanoclusters shape on the polarization switching and domain nucleation emerging in otherwise non-switchable piezoelectric films due to the proximity of ferroelectric nanoclusters. The boundary of the ferroelectric nanocluster embedded in the piezoelectric film is a compositionally graded layer.

We reveal that the proper choice of the cluster shape allows switching the electric polarization of the piezoelectric AlN film at coercive field significantly lower than the electric breakdown field due to the proximity of ferroelectric  $\text{Al}_{1-x}\text{Sc}_x\text{N}$  clusters. In particular, the inclusion of spike-like  $\text{Al}_{0.73}\text{Sc}_{0.27}\text{N}$  clusters reduces the coercive field of the AlN film strongest of all (~1.56 times compared to pure AlN film). The inclusion of semi-circular  $\text{Al}_{0.73}\text{Sc}_{0.27}\text{N}$  clusters leads to smaller reduction of the coercive field; and the inclusion of flattened  $\text{Al}_{0.73}\text{Sc}_{0.27}\text{N}$  clusters reduces the coercive field weakest of all (~1.04 times compared to AlN film).

We also explored the underlaying physical mechanisms of the proximity effects in the piezoelectric films with ferroelectric nanoclusters. The internal field, which is depolarizing inside the piezoelectric film (due to the larger spontaneous polarization of AlN) and polarizing in the ferroelectric cluster (due to the smaller spontaneous polarization of  $\text{Al}_{0.73}\text{Sc}_{0.27}\text{N}$ ), lowers the potential barrier and facilitates the nucleation of nanodomains in the clusters. Next stages, namely the instant vertical growth of nanodomains to the bottom electrode and their lateral growth in the piezoelectric film, appear due to the proximity effect.

We also analyzed the polarization switching in the inverted structures, where we varied the shape of AlN clusters in the  $\text{Al}_{1-x}\text{Sc}_x\text{N}$  film. We revealed that the AlN clusters with semi-circular cross-section reduce the coercive field strongest of all other shapes of the cross-sections. In result, the coercive field appears smaller (up to ~1.22 times) than the field of pure  $\text{Al}_{0.73}\text{Sc}_{0.27}\text{N}$  film. In this case, the internal field, which is polarizing inside the  $\text{Al}_{0.73}\text{Sc}_{0.27}\text{N}$  film and depolarizing in the AlN cluster, lowers the potential barrier in the film and facilitates the nucleation of nanodomains outside the AlN clusters, in the immediate vicinity of cluster-electrode contacts, which act as polar interfacial defects. Next stages, which are the vertical growth of needle-like nanodomains towards the bottom electrode and their lateral growth in the film and in the AlN clusters, occur due to the proximity effect.

Since considered nanostructured materials can be created by implantation of Sc ions into AlN films, obtained theoretical results can be useful for creation of nanopatterned ferroelectrics by chemical engineering, with exciting prospects for previously unrealizable ferroelectric memory technologies.

**Acknowledgements.** The work of A.N.M. and E.A.E. is funded by the National Academy of Sciences of Ukraine and (in part) by the DOE Software Project on “Computational Mesoscale Science and Open Software for Quantum Materials”, under Award Number DE-SC0020145 as part of the Computational Materials Sciences Program of US Department of Energy, Office of Science, Basic Energy Sciences. The work of L.Q.C. and V.G. are sponsored by the DOE Software Project on “Computational Mesoscale Science and Open Software for Quantum Materials”, under Award Number DE-SC0020145 as part of the Computational Materials Sciences Program of US Department of Energy, Office of Science, Basic Energy Sciences. The work of S.V.K. is supported by S.V.K. start-up funds. Results were visualized in Mathematica 14.0 [33].

**Authors' contribution.** A.N.M. and V.G. generated the research idea. A.N.M. formulated the problem, suggested mathematical model, analyzed obtained results and wrote the manuscript draft. E.A.E. wrote the codes and performed numerical modelling. S.V.K., L.Q.C., D.R.E., and V.G. worked on results explanation and manuscript improvement.

## Supplementary Materials to the Manuscript

LGD parameters of  $\text{Al}_{0.73}\text{Sc}_{0.27}\text{N}$  and AlN, used in the FEM, are listed in **Table SI**. The LGD parameters of  $\text{Al}_{0.73}\text{Sc}_{0.27}\text{N}$  were determined from the experimentally measured spontaneous polarization [34, 35] and linear dielectric permittivity [36] as described in Refs. [37] and [38]. The background permittivity  $\varepsilon_b$  is estimated as the square of refractive index according to Ref. [39]. Also, we assume equal gradient tensor coefficients in longitudinal and transverse directions,  $g_{z,\perp}^{(i)} = 1.0 \cdot 10^{-10} \text{ m}^3/\text{F}$ .

**Table SI.** LGD model parameters of  $\text{Al}_{0.73}\text{Sc}_{0.27}\text{N}$  and AlN. Adapted from Ref. [24].

compound	$\alpha_i, \text{m/F}$	$\beta_i, \text{m}^5/(\text{F C}^2)$	$\gamma_i, \text{m}^7/(\text{F C}^4)$	$E_c^{\text{bulk}}, \text{MV/cm}^*$	$\varepsilon_b^{(i)} \approx \varepsilon_{11}^{(i)}$
AlN layer	$-2.164 \cdot 10^9$	$-3.155 \cdot 10^9$	$2.788 \cdot 10^9$	26.1	4
$\text{Al}_{0.73}\text{Sc}_{0.27}\text{N}$	$-2.644 \cdot 10^8$	$-3.155 \cdot 10^9$	$2.788 \cdot 10^9$	9.3	3

\* The thermodynamic coercive field of a stress-free bulk material

Electrostriction coefficients  $Q_{ij}$  and elastic stiffness  $c_{ij}$  tensors components of ferroelectric and piezoelectric layers, which are regarded the same, are collected from Refs. [40, 41]. They are listed in **Table S2**.

**Table S2.** Elastic parameters of AlN and  $\text{Al}_{0.73}\text{Sc}_{0.27}\text{N}$ . Adapted from Ref. [24].

parameters	$Q_{ij}$ , $\text{m}^4/\text{C}^2$	Ref.	$c_{ij}$ , GPa	Ref.
AlN	$Q_{13} = -0.0087$ , $Q_{33} = 0.0203$	[40]	$c_{11}=396$ , $c_{12}=137$ , $c_{13} = 108$ , $c_{33} = 373$ , $c_{44} = 116$ , $c_{66} = 130$	[42]
$\text{Al}_{0.73}\text{Sc}_{0.27}\text{N}$	$Q_{13} = -0.0152$ , $Q_{33} = 0.0406$	[40]	$c_{11}=319$ , $c_{12}=151$ , $c_{13} = 127$ , $c_{33} = 249$ , $c_{44} = 101$ , $c_{66} = 84$	[42]

## References

[1] T. Mikolajick, S. Slesazeck, H. Mulaosmanovic, M. H. Park, S. Fichtner, P. D. Lomenzo, M. Hoffmann, U. Schroeder. Next generation ferroelectric materials for semiconductor process integration and their applications, *J. Appl. Phys.* **129**, 100901 (2021), <https://doi.org/10.1063/5.0037617>

[2] K.-H. Kim, I. Karpov, R. H. Olsson III, D. Jariwala. Wurtzite and fluorite ferroelectric materials for electronic memory, *Nature Nanotechnology* **18**, 422 (2023), <https://doi.org/10.1038/s41565-023-01361-y>

[3] K. P. Kelley, A. N. Morozovska, E. A. Eliseev, Y. Liu, S. S. Fields, S. T. Jaszewski, T. Mimura, J. F. Ihlefeld, S. V. Kalinin. Ferroelectricity in Hafnia Controlled via Surface Electrochemical State. *Nature Materials* **22**, 1144 (2023), <https://doi.org/10.1038/s41563-023-01619-9>

[4] S. Fichtner, N. Wolff, F. Lofink, L. Kienle, and B. Wagner. AlScN: A III-V semiconductor based ferroelectric, *Journal Applied Physics* **125**, 114103 (2019); <https://doi.org/10.1063/1.5084945>

[5] W. Zhu, J. Hayden, F. He, J.-I. Yang; P. Tipsawat, M. D. Hossain, J.-P. Maria, and S. Trolier-McKinstry. Strongly temperature dependent ferroelectric switching in AlN,  $\text{Al}_{1-x}\text{Sc}_x\text{N}$ , and  $\text{Al}_{1-x}\text{B}_x\text{N}$  thin films. *Applied Physics Letters* **119**, 062901 (2021); <https://doi.org/10.1063/5.0057869>

[6] Y. Gu, A. C. Meng, A. Ross, and L.-Q. Chen. A phenomenological thermodynamic energy density function for ferroelectric wurtzite  $\text{Al}_{1-x}\text{Sc}_x\text{N}$  single crystals, *J. Appl. Phys.* **135**, 094102 (2024), <https://doi.org/10.1063/5.0190677>

[7] P. Chen, D. Wang, A. M. Tejerina, K. Yazawa, A. Zakutayev, C. Paillard, L. Bellaiche. Towards a deeper fundamental understanding of (Al,Sc)N ferroelectric nitrides (2025); <https://doi.org/10.48550/arXiv.2509.1505>

[8] M. H. Park, C.-C. Chung, T. Schenk, C. Richter, K. Opsomer, C. Detavernier, C. Adelmann, J.L. Jones, T. Mikolajick, U. Schroeder. Effect of Annealing Ferroelectric  $\text{HfO}_2$  Thin Films: In Situ, High Temperature X-Ray Diffraction. *Advanced Electronic Materials* **4**, 1800091 (2018), <https://doi.org/10.1002/aelm.201800091>

[9] M. Saadi, et al. Exploring the underlying mechanisms of ferroelectric behavior in metal-doped aluminum nitride: an in-depth review. *Microstructures*, **5**, 2025092 (2025); <https://dx.doi.org/10.20517/microstructures.2024.136>

---

[10] F. Yang. Physics of Ferroelectric Wurtzite  $\text{Al}_{1-x}\text{Sc}_x\text{N}$  Thin Films. *Adv. Electron. Mater.*, **11**, 2400279 (2025); <https://doi.org/10.1002/aelm.202400279>

[11] J. Zhang, Z. Pan, Y. Guo, M. Chu, M. Quddamah Khokhar, and J. Yi.  $\text{Al}_{1-x}\text{B}_x\text{N}$  Ferroelectric Thin Films: Research Progress and Prospects for Engineering Applications. *Phys. Status Solidi A*, **e202500561** (2025); <https://doi.org/10.1002/pssa.202500561>

[12] J. Yang, A. V. Ievlev, A. N. Morozovska, E. Eliseev, J. D Poplawsky, D. Goodling, R. J. Spurling, J.-P. Maria, S. V. Kalinin, Y. Liu. Coexistence and interplay of two ferroelectric mechanisms in  $\text{Zn}_{1-x}\text{Mg}_x\text{O}$ . *Advanced Materials* **36**(39), 2404925 (2024), <https://doi.org/10.1002/adma.202404925>

[13] Wolff, N., Schönweger, G., Streicher, I., Islam, M.R., Braun, N., Straňák, P., Kirste, L., Prescher, M., Lotnyk, A., Kohlstedt, H. and Leone, S., Demonstration and STEM Analysis of Ferroelectric Switching in MOCVD-Grown Single Crystalline  $\text{Al}_{0.85}\text{Sc}_{0.15}\text{N}$ . *Advanced Physics Research*, **2300113** (2024), <https://doi.org/10.1002/apxr.202300113>

[14] W. Zhu, J. Hayden, F. He, J.I. Yang, P. Tipsawat, M.D. Hossain, J.P. Maria, and S. Trolier-McKinstry. Strongly temperature dependent ferroelectric switching in  $\text{AlN}$ ,  $\text{Al}_{1-x}\text{Sc}_x\text{N}$ , and  $\text{Al}_{1-x}\text{B}_x\text{N}$  thin films, *Appl. Phys. Lett.* **119**, 062901 (2021), <https://doi.org/10.1063/5.0057869>

[15] Y. Liu, A. V. Ievlev, E. A. Eliseev, A. M. Dinani, A. Sepehrinezhad, U. S. Hassan, D. Behrendt, N. Sun, K. Okamoto, H. Funakubo, A. M. Rappe, A. C. T. van Duin, A. N. Morozovska, S. Kalinin. Polarization switching on the open surfaces of the wurtzite ferroelectric nitrides: ferroelectric subsystems and electrochemical reactivity. *Advanced Materials* (2025); <https://doi.org/10.1002/adma.202511001>

[16] V. Gopalan, and T. E. Mitchell. In situ video observation of 180 domain switching in  $\text{LiTaO}_3$  by electro-optic imaging microscopy. *J. Appl. Phys.* **85**, 2304 (1999), <https://doi.org/10.1063/1.369542>

[17] C. H. Skidmore, R. J. Spurling, J. Hayden, S. M. Baksa, D. Behrendt, D. Goodling, J. L. Nordlander, A. Suceava, J. Casamento, B. Akkopru-Akgun, S. Calderon, I. Dabo, V. Gopalan, K. P. Kelley, A. M. Rappe, S. Trolier-McKinstry, E. C. Dickey & J.-P. Maria. Proximity ferroelectricity in wurtzite heterostructures, *Nature*, (2024), <https://doi.org/10.1038/s41586-024-08295-y>

[18] E. A. Eliseev, A. N. Morozovska, J.-P. Maria, L.-Q. Chen, and V. Gopalan. A Thermodynamic Theory of Proximity Ferroelectricity. *Physical Review X*, **15**, 021058 (2025), <https://doi.org/10.1103/PhysRevX.15.021058>

[19] E. A. Eliseev, A. N. Morozovska, S. V. Kalinin, L.-Q. Chen, and V. Gopalan. Tip-Based Proximity Ferroelectric Switching and Piezoelectric Response in Wurtzite Multilayers. *Physical Review Applied* **24**, 054026 (2025); <https://link.aps.org/doi/10.1103/plhw-fkk9>

[20] Z-G. Ban, S. P. Alpay, and J. V. Mantese. Fundamentals of graded ferroic materials and devices. *Physical Review B* **67**, 184104 (2003); <https://doi.org/10.1103/PhysRevB.67.184104>

[21] Z.G. Ban, S.P. Alpay, J.V. Mantese, Hysteresis offset and dielectric response of compositionally graded ferroelectric materials. *Integrated Ferroelectrics*, **58**(1), 1281 (2003); <https://doi.org/10.1080/10584580390259470>

---

[22] G. Akcay, S. Zhong, B. S. Allimi, S. P. Alpay, and J. V. Mantese. Strain induced internal potentials of compositionally graded epitaxial ferroelectric thin films. *Applied Physics Letters* **91**, 012904 (2007). <https://doi.org/10.1063/1.2754358>

[23] I.B. Misirlioglu and S.P. Alpay. Compositionally graded ferroelectrics as wide band gap semiconductors: Electrical domain structures and the origin of low dielectric loss. *Acta Materialia* **122**, 266-276 (2017); <https://doi.org/10.1016/j.actamat.2016.09.050>

[24] E. A. Eliseev, A. N. Morozovska, S. V. Kalinin, L.-Q. Chen, and V. Gopalan. Proximity Ferroelectricity in Compositionally Graded Structures (2025); <https://doi.org/10.48550/arXiv.2509.13443>

[25] Eriksson, K.; Estep, D.; Johnson, C. (2004). *Applied mathematics, body and soul*. Berlin; New York: Springer. ISBN 3-540-00889-6.

[26] C.L. Jia, V. Nagarajan, J.Q. He, L. Houben, T. Zhao, R. Ramesh, K. Urban, R. Waser, Unit-cell scale mapping of ferroelectricity and tetragonality in epitaxial ultrathin ferroelectric films, *Nature materials* **6**, 64 (2007); <https://doi.org/10.1038/nmat1808>

[27] A. K. Tagantsev and G. Gerra. Interface-induced phenomena in polarization response of ferroelectric thin films. *J. Appl. Phys.* **100**, 051607 (2006). <https://doi.org/10.1063/1.2337009>

[28] See Supplementary Materials for details [URL will be provided by Publisher]

[29] S. Fichtner, N. Wolff, G. Krishnamurthy, A. Petraru, S. Bohse, F. Lofink, S. C. H. Kohlstedt, L. Kienle, and B. Wagner. Identifying and overcoming the interface originating c-axis instability in highly Sc enhanced AlN for piezoelectric micro-electromechanical systems. *J. of Appl. Phys.* **122**, 035301 (2017), <https://doi.org/10.1063/1.4993908>

[30] N. Watanabe, T. Kimoto, and J. Suda. The temperature dependence of the refractive indices of GaN and AlN from room temperature up to 515 °C. *J. Appl. Phys.* **104**, 106101 (2008), <https://doi.org/10.1063/1.3021148>

[31] O. Ambacher, B. Christian, N. Feil, D. F. Urban, C. Elsässer, M. Prescher, and L. Kirste. Wurtzite ScAlN, InAlN, and GaAlN crystals, a comparison of structural, elastic, dielectric, and piezoelectric properties, *J. Appl. Phys.* **130**, 045102 (2021); <https://doi.org/10.1063/5.0048647>

[32] A. N. Morozovska, O. V. Bereznykov, M. V. Strikha, O. S. Pylypchuk, Z. Kutnjak, E. A. Eliseev, and D. R. Evans. Domain Morphology, Electrocaloric Response, and Negative Capacitance States of Ferroelectric Nanowires Array. *Composite Interfaces* (2025); <https://doi.org/10.1080/09276440.2025.2605389>

[33] <https://www.wolfram.com/mathematica>, <https://notebookarchive.org/2024-06-bhmuw2b>

[34] S. Fichtner, N. Wolff, F. Lofink, L. Kienle, and B. Wagner. AlScN: A III-V semiconductor based ferroelectric, *J. Appl. Phys.* **125**, 114103 (2019), <https://doi.org/10.1063/1.5084945>

[35] W. Zhu, J. Hayden, F. He, J.I. Yang, P. Tipsawat, M.D. Hossain, J.P. Maria, and S. Trolier-McKinstry. Strongly temperature dependent ferroelectric switching in AlN, Al<sub>1-x</sub>Sc<sub>x</sub>N, and Al<sub>1-x</sub>B<sub>x</sub>N thin films, *Appl. Phys. Lett.* **119**, 062901 (2021), <https://doi.org/10.1063/5.0057869>

[36] S. Fichtner, N. Wolff, G. Krishnamurthy, A. Petraru, S. Bohse, F. Lofink, S. C., H. Kohlstedt, L. Kienle, and B. Wagner. Identifying and overcoming the interface originating c-axis instability in highly Sc

---

enhanced AlN for piezoelectric micro-electromechanical systems. *J. of Appl. Phys.* **122**, 035301 (2017), <https://doi.org/10.1063/1.4993908>

[37] Y. Gu, A. C. Meng, A. Ross, and L.-Q. Chen. A phenomenological thermodynamic energy density function for ferroelectric wurtzite  $\text{Al}_{1-x}\text{Sc}_x\text{N}$  single crystals, *J. Appl. Phys.* **135**, 094102 (2024), <https://doi.org/10.1063/5.0190677>

[38] E. A. Eliseev, A. N. Morozovska, J.-P. Maria, L.-Q. Chen, and V. Gopalan. A Thermodynamic Theory of Proximity Ferroelectricity. *Physical Review X*, **15**, 021058 (2025), <https://doi.org/10.1103/PhysRevX.15.021058>

[39] N. Watanabe, T. Kimoto, and J. Suda. The temperature dependence of the refractive indices of GaN and AlN from room temperature up to 515 °C. *J. Appl. Phys.* **104**, 106101 (2008), <https://doi.org/10.1063/1.3021148>

[40] Y. Gu, A. C. Meng, A. Ross, and L.-Q. Chen. A phenomenological thermodynamic energy density function for ferroelectric wurtzite  $\text{Al}_{1-x}\text{Sc}_x\text{N}$  single crystals, *J. Appl. Phys.* **135**, 094102 (2024), <https://doi.org/10.1063/5.0190677>

[41] O. Ambacher, B. Christian, N. Feil, D. F. Urban, C. Elsässer, M. Prescher, and L. Kirste. Wurtzite ScAlN, InAlN, and GaAlN crystals, a comparison of structural, elastic, dielectric, and piezoelectric properties, *J. Appl. Phys.* **130**, 045102 (2021); <https://doi.org/10.1063/5.0048647>

[42] O. Ambacher, B. Christian, N. Feil, D. F. Urban, C. Elsässer, M. Prescher, and L. Kirste. Wurtzite ScAlN, InAlN, and GaAlN crystals, a comparison of structural, elastic, dielectric, and piezoelectric properties, *J. Appl. Phys.* **130**, 045102 (2021); <https://doi.org/10.1063/5.0048647>